Journal of Power Sources 246 (2014) 906–911

Contents lists available at ScienceDirect

Journal of Power Sources

journal homepage: www.elsevier.com/locate/jpowsour

Characterization of $SrFe_{0.75}Mo_{0.25}O_{3-\delta}$–$La_{0.9}Sr_{0.1}Ga_{0.8}Mg_{0.2}O_{3-\delta}$ composite cathodes prepared by infiltration

Xie Meng, Da Han, Hao Wu, Junliang Li*, Zhongliang Zhan*

CAS Key Laboratory of Materials for Energy Conversion, Shanghai Institute of Ceramics, Chinese Academy of Sciences (SICCAS), 1295 Dingxi Road, Shanghai 200050, China

HIGHLIGHTS

- $SrFe_{0.75}Mo_{0.25}O_{3-\delta}$–$La_{0.9}Sr_{0.1}Ga_{0.8}Mg_{0.2}O_{3-\delta}$ composites are fabricated using the liquid phase impregnation method.
- The nano-scale $SrFe_{0.75}Mo_{0.25}O_{3-\delta}$ cathodes exhibit area specific resistances of 0.04 Ω cm^2 in air at 800 °C.
- Impedance analysis shows that ionization of adsorbed oxygen is the rate-limiting step for oxygen reduction reactions.

ARTICLE INFO

Article history:
Received 14 March 2013
Received in revised form
10 August 2013
Accepted 12 August 2013
Available online 28 August 2013

Keywords:
Solid oxide fuel cells
Strontium and magnesium doped lanthanum gallate
Molybdenum doped strontium ferrite
Cathodes
Impregnation

ABSTRACT

This paper describes the structure and electrochemical properties of composite cathodes for solid oxide fuel cells fabricated by infiltration of aqueous solutions corresponding to $SrFe_{0.75}Mo_{0.25}O_{3-\delta}$ (SFMO) into porous $La_{0.9}Sr_{0.1}Ga_{0.8}Mg_{0.2}O_{3-\delta}$ (LSGM) backbones. XRD measurement confirms the predominance of the perovskite SFMO oxides in the infiltrates together with some minor impurities of $SrMoO_4$ after calcinations at 850–1100 °C. The cathode polarization resistance as obtained from impedance measurement on symmetric cathode fuel cells exhibits a pronounced increase as a function of calcinations temperature due to increased SFMO particle sizes, *e.g.*, 0.04 Ω cm^2 for 70 nm-sized catalysts calcinated at 850 °C *versus* 0.11 Ω cm^2 for 400 nm-sized catalysts calcinated at 1100 °C. Oxygen partial pressure and temperature dependence of impedance data shows that oxygen reduction kinetics is largely determined by ionization of adsorbed oxygen atoms on the SFMO catalysts.

1. Introduction

The solid oxide fuel cell (SOFC) provides a clean and efficient approach for electrochemically converting fuels into electricity, and consists of a porous anode and a porous cathode separated by a gas-impermeable electrolyte [1]. In order to reduce interfacial polarization resistances and deliver high power outputs, high catalytic activities are required for both electrodes, especially for the cathodes that are usually fabricated via calcinations at high temperatures that yield porous structures at micron scales [2,3]. Due to their superior catalytic activities, nanocrystalline and nanoporous materials have received continuously increased interest as the active cathode catalysts for intermediate temperature SOFCs operating over the regime of 500–800 °C [4–10]. Liu et al. reported pulse laser deposition of nanostructured $Ba_{0.5}Sr_{0.5}Co_{0.8}Fe_{0.2}O_{3-\delta}$ (BSCF) cathodes with an average particle size of 40 nm on the yttrium-stabilized zirconia (YSZ) electrolytes, which allowed for much higher power densities than obtainable with the micron-scale BSCF cathodes prepared using the screen-printing method followed by calcinations at high temperatures [11]. Nanoporous $La_{0.6}Sr_{0.4}CoO_{3-\delta}$ thin-film cathodes with an average grain size of 17 nm were deposited by a sol–gel technique on the $Ce_{0.9}Gd_{0.1}O_{1.95}$ electrolytes, producing a low area specific resistance of 0.023 Ω cm^2 at 600 °C [12]. Liquid phase infiltration is a relatively new approach for preparing nanostructured SOFC cathodes, where well-interconnected and nano-scale oxide catalyst coatings are supported on the internal surfaces of micron-scale porous backbones [13]. In particular, infiltration of perovskite oxides with mixed ionic and electronic conductivities into the high ionic-conductivity backbones yielded composite cathodes that showed very low polarization resistances ($R_{P,C}$) due to enlarged area available for surface oxygen exchange. For example, the $R_{P,C}$ value of 0.1 Ω cm^2 were

* Corresponding authors. Tel./fax: +86 21 6990 6373.
E-mail addresses: ljl2005@mail.sic.ac.cn (J. Li), zzhan@mail.sic.ac.cn (Z. Zhan).

0378-7753/$ – see front matter © 2013 Elsevier B.V. All rights reserved.
http://dx.doi.org/10.1016/j.jpowsour.2013.08.057

achieved for the composite cathodes of $La_{0.8}Sr_{0.2}FeO_{3-\delta}$ infiltrated YSZ [14], $Sm_{0.5}Sr_{0.5}CoO_{3-\delta}$ (SSC) infiltrated GDC [15] and SSC infiltrated LSGM [10] at 700, 600 and 550 °C, respectively. Simultaneous infiltration of $Ce_{0.8}Sm_{0.2}O_{1.9}$ (SDC) in addition to SSC in the LSGM backbones yielded smaller particle sizes by suppressing agglomeration and coarsening of SSC nanoparticles during the repeated infiltration/calcination cycles that facilitated surface oxygen exchange and thereby produced even lower $R_{P,C}$ values, *e.g.*, 0.075 Ω cm^2 at 550 °C and 0.137 Ω cm^2 at 500 °C [16].

Up to date, the infiltrated cathode catalysts have been mainly focused upon the cobalt-containing perovskite oxides due to their high electrical conductivities and the intermediate-spin state of the surface Co(III) that promotes reduction of adsorbed gaseous O_2 to surface O^{2-}. Nevertheless, the cobalt-based materials showed poor chemical stability in the presence of CO_2 and in a strongly reducing atmosphere around the triple-phase boundaries when fuel cells are operated at low voltages. In addition, increased stability of the cathode material in reducing atmospheres is also preferable for single-chamber [17,18], direct-flame [19] and metal-supported SOFCs [20] from the perspectives of long-term durability and fabrication easiness. Recent, Liu and Xiao reported that the Mo-doped $SrFeO_{3-\delta}$ perovskite oxides were redox-stable and showed great promise as a new cathode material for intermediate temperature SOFCs [21,22]. In the present paper, the $SrFe_{0.75}Mo_{0.25}O_{3-\delta}$ (SFMO) cathodes were fabricated by infiltration into the porous LSGM backbones, and the catalytic activity of the resulting composites for oxygen reduction reactions was evaluated via impedance measurement on the symmetric cathode fuel cells. The effect of the calcinations temperature on the microstructure and the catalytic activity of the SFMO–LSGM composite cathodes were described and the oxygen reduction kinetics was briefly discussed.

2. Experimental

The SFMO–LSGM composite cathodes were fabricated based upon an LSGM tri-layer structure—a 15 μm thick dense layer sandwiched between two 150 μm-thick porous layers, which was obtained by laminating three tape-cast ceramic green tapes with rice starch as the fugitive material for the porous layers. Powders of LSGM (5 m^2 g^{-1}, Praxair) and rice starch were ball-milled in a weight ratio of 60:40 for 24 h with appropriate amounts of dispersant, binder, plasticizer and solvent. After de-air in vacuum for ≈10 min, the slurry was cast on a polyethylene film under the doctor blade. The resulting green tapes of porous LSGM layers were ≈90 μm. Green tapes of dense LSGM electrolyte were similarly prepared with a typically thickness of ≈20 μm except that no pore former was used in the tape casting formulation. One sheet of dense LSGM tape and two sheets of porous LSGM tapes on each side were uniaxially laminated at 75 °C for 10 min under a pressure of 3000 psi, which were then co-sintered at 1450 °C for 6 h in order to densify the LSGM electrolyte layer.

The perovskite oxides of SFMO were added by infiltrating an aqueous solution containing $Sr(NO_3)_2$, $Fe(NO_3)_3{\cdot}9H_2O$, $(NH_4)_6Mo_7O_{24}{\cdot}4H_2O$ and citric acid in a molar ratio of 1:0.75:0.0357:2 into the porous LSGM backbones, followed by calcinations at 850, 1000 and 1100 °C for 2 h. The resulting composites were designated as SFMO850, SFMO1000 and SFMO1100, respectively. All these chemicals were 99% pure and purchased from Sinopharm Chemical Reagent. The quantity of the deposited SFMO catalysts was estimated by the weight difference before and after each infiltration/calcinations cycle, and multiple infiltration/calcinations cycles were used to introduce a sufficient amount of SFMO catalysts into the LSGM backbones. The phase composition of the resulting infiltrate was examined by X-ray diffraction (XRD) using a monochromatic Cu K_α radiation source.

The catalytic activity of the SFMO–LSGM composite cathodes was evaluated on the symmetric cathode fuel cells via impedance measurement over the temperature range of 600–800 °C. Silver ink was applied on the electrode surface as the current collector and silver wires were used as the voltage and current leads. The impedance spectra were obtained at open circuits in ambient air or oxygen balanced by nitrogen using an IM6 Electrochemical Workstation (ZAHNER, Germany) over the frequency range from 0.1 Hz to 200 kHz with a 20 mV ac perturbation. The cell structure was examined using scanning electron microscopy (SEM) in a Hitachi S-4800-II microscope.

3. Results and discussion

For the composite cathodes prepared by the liquid infiltration technique, the infiltrates catalyze oxygen reduction reactions and simultaneously collect the electrical current. Formation of the electrically conducting SFMO perovskite oxides is critically important for obtaining high performance composite cathodes. X-ray diffraction (XRD) was thereby used to examine the phase compositions of the infiltrates as a function of calcination temperature. Fig. 1 shows the typical XRD results for a 25 wt% SFMO infiltrated LSGM composites calcinated at 850 and 1100 °C that confirmed the predominant presence of the perovskite oxides in the infiltrates. Formation of the SFMO catalysts was further confirmed by an independent XRD analysis of SFMO–YSZ composite electrodes that were obtained in the same manner (Fig. 1b).

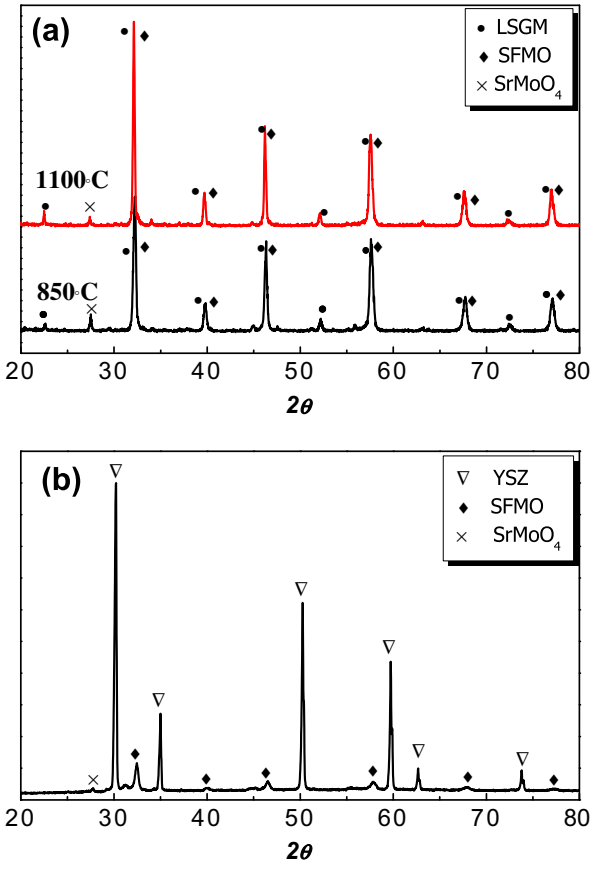

Fig. 1. The X-ray diffraction patterns of (a) SFMO–LSGM and (b) SFMO–YSZ composites.

Note that some minor impurities of $SrMoO_4$ were also observed and probably resulted from the melted intermediate oxide of MoO_3 (melting point: 795 °C) that would produce phase inhomogenity [23]. This is consistent with prior reports that repeated grindings and calcinations are required to obtain phase-pure SFMO oxides [24]. Comparison of XRD patterns shown in Fig. 1a indicates that increasing the calcination temperature from 850 °C to 1100 °C reduced the amount of $SrMoO_4$ impurities present in the infiltrates as evidenced by the decreased diffraction peak at 27.4°.

The morphology and microstructure of the infiltrated SFMO coatings calcinated at different temperatures were examined by SEM, with the representative micrographs shown in Fig. 2. Porosities in LSGM backbones resulted from the use of 40 wt% starch as the fugitive material in the tape casting formulation. Mercury porosimetry measurements of the porous LSGM backbones showed a bi-modal distribution respectively centered at 1 and 6 μm with overall porosities of 45%. Notably, a solid loading of 25 wt% was sufficient to form well-intraconnected coatings at all temperatures that is required for the composite cathodes to provide efficient current collection and enlarge the electrochemically active areas via reducing the portion of isolated catalysts [10]. Decreasing the loading increased the fraction of isolated catalyst particles while increasing the loading decreased the overall porosity of the impregnated composite, both of which resulted in increased polarization resistances as previously observed for alternative cathodes prepared in the same manner [10]. Fig. 2 also shows that the SFMO particles grew larger and the coatings tended to become more dense with increasing calcination temperature. Similar behavior has been previously observed for the composites of $La_{0.8}Sr_{0.2}FeO_3$, $LaNi_{0.6}Fe_{0.4}O_3$ or $La_{0.91}Sr_{0.09}Ni_{0.6}Fe_{0.4}O_3$ infiltrated YSZ [14,25]. Based upon these high-magnification SEM micrographs, the average particle sizes of the SFMO catalysts were estimated to be 70, 200 and 400 nm for SFMO850, SFMO1000 and SFMO1100, respectively.

Influence of the calcination temperature on the catalytic activities of the SFMO infiltrated LSGM composites is illustrated by Nyquist and Bode plots in Fig. 3 of impedance data, as obtained from measurement of symmetric cathode fuel cells in ambient air at 800 °C. The ohmic resistances primarily due to the electrolytes were removed and the non-ohmic resistances were divided by two so as to account for contributions of two symmetric cathodes. The Nyquist plot for SFMO850 consisted of two depressed arcs centered at 200 Hz and 2 Hz, respectively. The peak frequency associated with the higher-frequency process decreased continuously with increasing the calcination temperature, resulting in increased overlapping of the higher- and lower-frequency arcs in the Nyquist plots and thereby complicating deconvolution of the impedance data for SFMO1000 and SFMO1100. The total cathode polarization resistances at 800 °C, taken as the overall width of the arcs as shown in Fig. 3a, were 0.04, 0.07 and 0.11 Ω cm^2 for SFMO850, SFMO1000 and SFMO1100, respectively. Note that SFMO1000 and SFMO1100 exhibited polarization resistances comparable to the micron-scale SFMO cathodes prepared by the conventional screen-printing technique [22]. Much lower polarization resistance for SFMO850 than for SFMO1000 and SFMO1100 can be explained by the smaller particle size as shown in Fig. 2a and the resultant larger surface area available for oxygen reduction reactions [9]. Fig. 4 summarizes the total cathode polarization resistances at varied temperatures for SFMO850, SFMO1000 and SFMO1100, showing smaller polarization resistances at all measurement temperatures for the SFMO–LSGM composites calcinated at lower temperatures. In particular, the polarization resistances for SFMO850 ranged from 0.04 Ω cm^2 at 800 °C to 0.28 Ω cm^2 at 600 °C in air. These results also indicate that the presence of insulating $SrMoO_4$ minor impurities in the infiltrates did not adversely influence the catalytic activity of the SFMO–LSGM composites, especially given the fact that SFMO850 contained larger amount of impurities than SFMO1100. The activation energies for oxygen reduction reactions over SFMO850, SFMO1000 and SFMO1100 were 0.77, 1.11 and 1.19 eV, respectively.

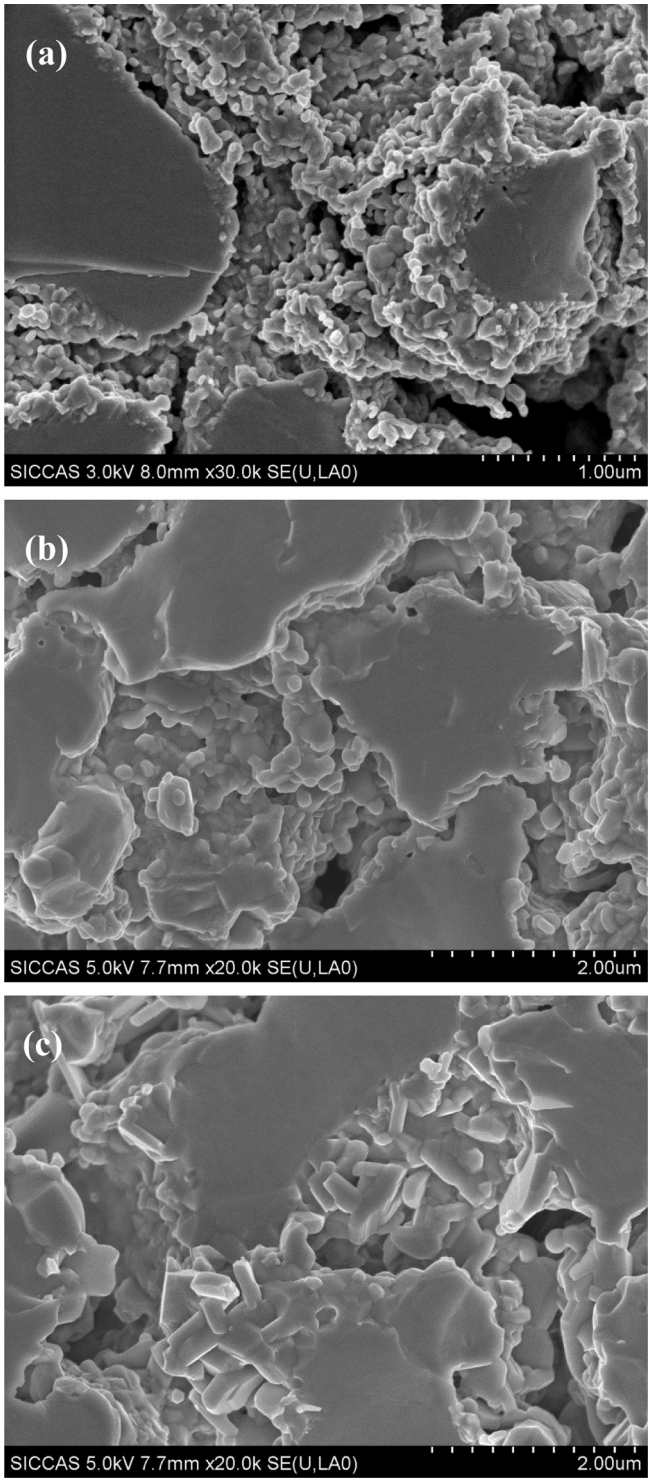

Fig. 2. The SEM micrograph of the SFMO–LSGM composite cathodes calcinated at (a) 850 °C, (b) 1000 °C and (c) 1100 °C.

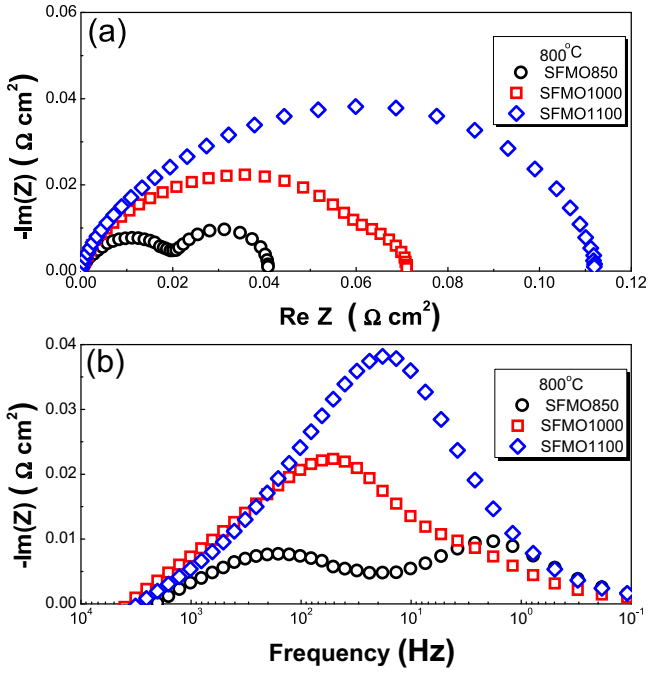

Fig. 3. Comparison of impedance data for symmetric SFMO–LSGM cathode fuel cells with SFMO catalysts calcinated at different temperatures: (a) Nyquist and (b) Bode plots.

Since SFMO850 exhibited the smallest polarization resistances and the highest catalytic activities for oxygen reduction reactions, further analysis was conducted on the impedance data that showed the least extent of overlapping between the higher- and lower-frequency arcs in the Nyquist plots. In particular, impedance measurement was performed at 750 °C in the N_2–O_2 gas mixtures with varied oxygen partial pressures in order to gain insights into oxygen reduction kinetics over SFMO850, and these impedance data are summarized in Fig. 5a for the Bode plots and in Fig. 5b for the Nyquist plots. At high oxygen partial pressures (*e.g.*, 1 or 0.75 atm), only one depressed arc with the peak frequency at ≈200 Hz was observed in the Nyquist plot, indicating that the lower-frequency

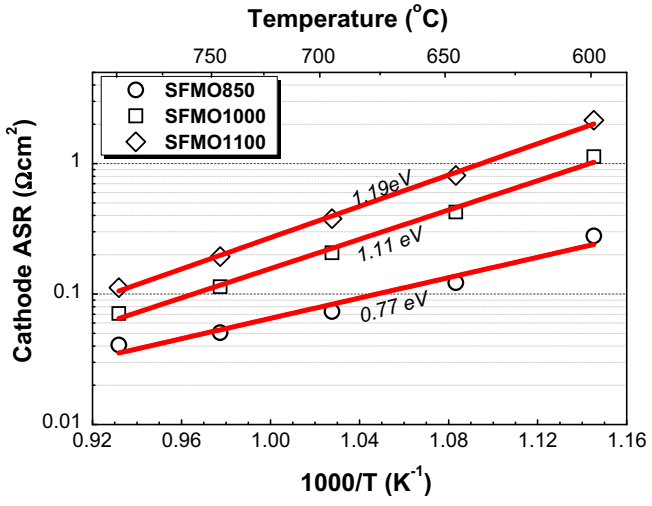

Fig. 4. The cathode polarization resistances plotted *versus* inverse temperature for SFMO–LSGM composites calcinated at different temperatures.

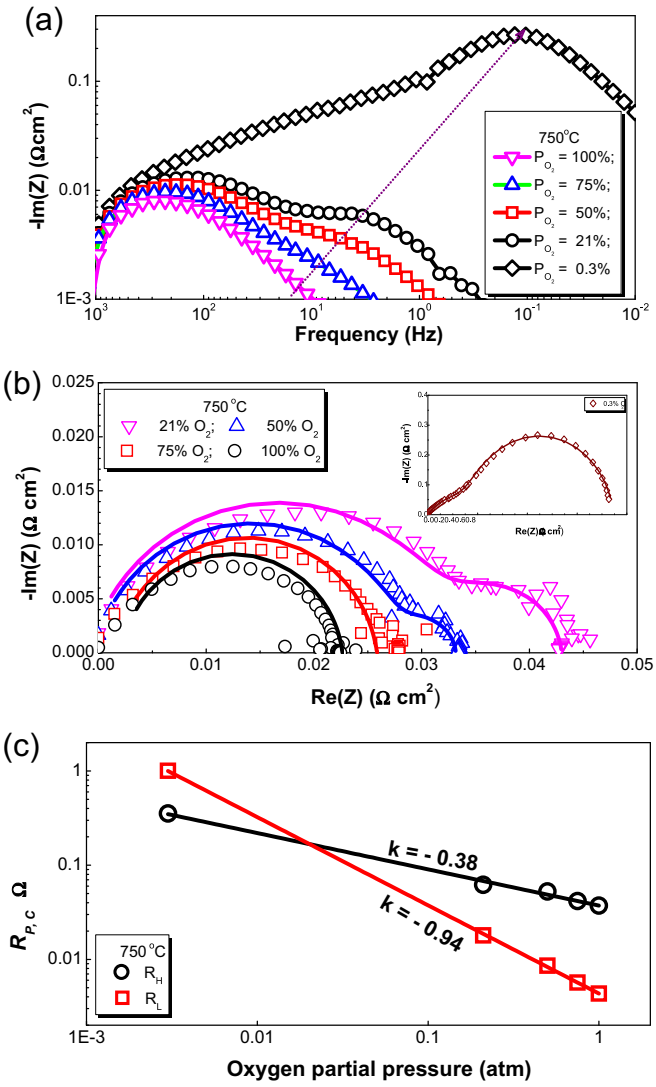

Fig. 5. (a) Bode and (b) Nyquist plots of impedance data for the symmetric fuel cells under varied oxygen partial pressures balanced by nitrogen. The equivalent circuits $LR_o(RQ)_h(RQ)_l$ was used to fit the impedance data at varied oxygen partial pressures. (c) Oxygen partial pressure dependence of the higher- and lower frequency arcs for impedance spectra in (b).

process was quick enough and the corresponding R_l resistance was too small to be distinguishable. With the oxygen partial pressure decreasing to 0.5 or 0.21 atm, the lower-frequency arc with the peak frequency at ≈2 Hz appeared in the Nyquist plots and was nevertheless much smaller than for the higher-frequency arc. Further decreasing the oxygen pressure down to 0.003 atm resulted in a dramatical increase in the lower-frequency arc that became dominant in the kinetics of oxygen reduction on SFMO850.

Fig. 5a and b also shows that the lower-frequency arc increased much more pronouncedly than the higher-frequency arc. These impedance data were fitted using a commonly used equivalent circuit, $LR_o(R_hQ_h)(R_lQ_l)$, where L was the conductance due to connecting wires, R_o was the pure ohmic resistance due to the electrolyte and the electrodes, R_h and R_l are the polarization resistances whereas Q_h and Q_l are the constant phase elements associated with the higher- and lower-frequecy process, respectively. Fig. 5c summarizes the resulting R_h and R_l values at varied oxygen pressures. Included in Fig. 5c are the fitting results using the equation $R_P \propto P_{O_2}^n$,

Table 1
Oxygen partial pressure dependence of the cathode polarization resistances ($R_P \propto P_{O_2}^n$) for varied rate-determining steps [26].

Rate-determining step	*n* values
$O_2(g) \rightarrow O_{2(ad)}$	−1
$O_{2(ad)} \rightarrow 2O_{ad}$	−0.5
$O_{ad} + e^- \rightarrow O_{ad}^-$	−0.375
$O_{ad}^- \rightarrow O_{TPB}^-$	−0.25
$O_{TPB}^- + e^- \rightarrow O_{TPB}^{2-}$	−0.125
$O_{TPB}^{2-} + V_O^{\cdot\cdot} \rightarrow O_O^{\times}$	0

where different *n* values reflect varied elementary steps in oxygen reduction reactions as summarized in Table 1 [26]. The fitted *n* values in Fig. 5c are −0.38 for R_h and −1 for R_l, in good agreement with prior results on the micron-sale SFMO cathodes [27]. Comparison of these *n* values with those in Table 1 indicates that the higher- and lower-frequency arcs are probably associated with ionization of adsorbed oxygen atom and non-dissociative adsorption of gaseous oxygen on the SFMO catalysts, respectively.

Fig. 6a shows the Nyquist plots for symmetric SFMO850 fuel cells measured in air at different temperatures, and the fitting results using the equivalent circuit $LR_o(R_hQ_h)(R_lQ_l)$ as discussed above were also included. Fig. 6b shows the R_h and R_l values for SFMO850 as a function of temperature. Due to the thermally-activated nature of ionization of adsorbed oxygen atom, the R_h value followed an Arrhenius dependence with an activation energy of 0.98 eV. On the other hand, the R_l value remained almost unaltered since non-dissociative adsorption of gaseous oxygen on the SFMO catalysts

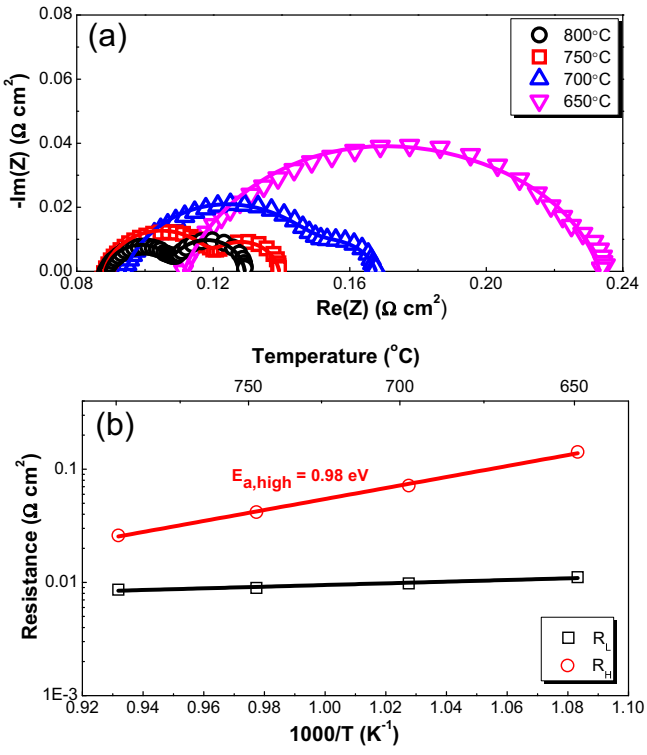

Fig. 6. (a) Nyquist plots of the impedance data at different temperatures for symmetric SFMO–LSGM cathode fuel cells with SFMO catalysts calcinated at 850 °C. The equivalent circuits $LR_o(RQ)_h(RQ)_l$ was used to fit the impedance data at varied temperatures. (b) Temperature dependence of the higher- and lower frequency arcs for impedance spectra in (a).

was largely temperature-independent. Much larger values for R_h than for R_l as shown in Fig. 6b indicate that ionization of adsorbed oxygen atom on the catalyst surfaces predominates oxygen reduction kinetics on the SFMO850 composites, as previously observed for the porous $La_{0.9}Sr_{0.2}Cr_{0.5}Mn_{0.5}O_{3-\delta}$ cathodes [28]. In other words, large surface area of the nanoporous structure and large surface exchange coefficient of oxygen over the SFMO catalysts enabled fast oxygen adsorption kinetics and thereby minimized the R_l value.

4. Conclusions

In summary, we have fabricated the non-randomly structured SFMO–LSGM composite cathodes by infiltrating nano-scale SFMO catalysts onto the internal surfaces of high-porosity LSGM backbones. Despite the presence of more $SrMoO_4$ minor impurities in the infiltrate coatings, the SFMO–LSGM composites calcinated at 850 °C exhibited substantially smaller polarization resistances in air than those calcinated at 1000 and 1100 °C. Analysis on oxygen partial pressure dependence of impedance data indicated that ionization of adsorbed oxygen atom was the rate-determining step for oxygen reduction reactions on the SFMO–LSGM composites calcinated at 850 °C while adsorption of gaseous oxygen was sufficiently fast on the surface of SFMO catalysts due to large surface area in the nanoporous coatings and high surface exchange coefficients of oxygen on the SFMO oxides.

Acknowledgments

The authors gratefully acknowledge the financial support of the National Basic Research Program of China under contract No. 2012CB215401, the National Science Foundation of China under contract No. 51072219, 51272272, 50902142, 51172266, Science and Technology Commission of Shanghai Municipality under contract No. 11PJ1410300, Science and Technology Commission of Zhejiang Province under contract No. 2011C16037, Chinese Government High Tech Developing Project under contract No. 2011AA050702, and the 100 Talents Program of Chinese Academy of Sciences.

References

[1] N.Q. Minh, J. Am. Ceram. Soc. 76 (1993) 563–588.
[2] A.J. Jacobson, Chem. Mater. 22 (2010) 660–674.
[3] C.W. Sun, R. Hui, J. Roller, J. Solid State Electrochem. 14 (2010) 1125–1144.
[4] Y. Liu, C. Compson, M.L. Liu, J. Power Sources 138 (2004) 194–198.
[5] J. Sacanell, A.G. Leyva, M.G. Bellino, D.G. Lamas, J. Power Sources 195 (2010) 1786–1792.
[6] J.M. Serra, S. Uhlenbruck, W.A. Meulenberg, H.P. Buchkremer, D. Stover, Top. Catal. 40 (2006) 123–131.
[7] J. Chen, F.L. Liang, L.N. Liu, S.P. Jiang, B. Chi, J. Pu, J. Li, J. Power Sources 183 (2008) 586–589.
[8] M. Darab, M.S. Toprak, G.E. Syvertsen, M. Muhammed, J. Electrochem. Soc. 156 (2009) K139–K143.
[9] Z.Y. Jiang, C.R. Xia, F.L. Chen, Electrochim. Acta 55 (2010) 3595–3605.
[10] D. Han, X.J. Liu, F.R. Zeng, J.Q. Qian, T.Z. Wu, Z.L. Zhan, Sci. Rep. 2 (2012).
[11] B. Liu, X.B. Chen, Y.L. Dong, S.S. Mao, M.J. Cheng, Adv. Energy Mater. 1 (2011) 343–346.
[12] L. Dieterle, P. Bockstaller, D. Gerthsen, J. Hayd, E. Ivers-Tiffee, U. Guntow, Adv. Energy Mater. 1 (2011) 249–258.
[13] J.M. Vohs, R.J. Gorte, Adv. Mater. 21 (2009) 943–956.
[14] Y.Y. Huang, J.M. Vohs, R.J. Gorte, J. Electrochem. Soc. 151 (2004) A646–A651.
[15] M. Shah, S.A. Barnett, Solid State Ionics 179 (2008) 2059–2064.
[16] Z.L. Zhan, D. Han, T.Z. Wu, X.F. Ye, S.R. Wang, T.L. Wen, S. Cho, S.A. Barnett, RSC Adv. 2 (2012) 4075–4078.
[17] Z.P. Shao, S.M. Haile, Nature 431 (2004) 170–173.
[18] Z.P. Shao, S.M. Haile, J. Ahn, P.D. Ronney, Z.L. Zhan, S.A. Barnett, Nature 435 (2005) 795–798.
[19] X.B. Zhu, B. Wei, Z. Lu, L. Yang, X.Q. Huang, Y.H. Zhang, M.L. Liu, Int. J. Hydrogen Energy 37 (2012) 8621–8629.
[20] M.C. Tucker, J. Power Sources 195 (2010) 4570–4582.

[21] Q.A. Liu, X.H. Dong, G.L. Xiao, F. Zhao, F.L. Chen, Adv. Mater. 22 (2010) 5478–5482.
[22] G.L. Xiao, Q. Liu, S.W. Wang, V.G. Komvokis, M.D. Amiridis, A. Heyden, S.G. Ma, F.L. Chen, J. Power Sources 202 (2012) 63–69.
[23] A.B. Munoz-Garcia, D.E. Bugaris, M. Pavone, J.P. Hodges, A. Huq, F.L. Chen, H.C. zur Loye, E.A. Carter, J. Am. Chem. Soc. 134 (2012) 6826–6833.
[24] J. Rager, A. Zipperle, A. Sharma, J.L. MacManus-Driscoll, J. Am. Ceram. Soc. 87 (2004) 1330–1335.
[25] S. Lee, M. Bevilacqua, P. Fornasiero, J.M. Vohs, R.J. Gorte, J. Power Sources 193 (2009) 747–753.
[26] A.A. M.J Escudero, J.A. Alonso, L. Daza, J. Electroanal. Chem. 611 (2007) 107–116.
[27] G.L. Xiao, Q.A. Liu, F. Zhao, L. Zhang, C.R. Xia, F.L. Chen, J. Electrochem. Soc. 158 (2011) B455–B460.
[28] Y. Zheng, C. Zhang, R. Ran, R. Cai, Z.P. Shao, D. Farrusseng, Acta Mater. 57 (2009) 1165–1175.